EUV free-standing transmittance filters based on Nb/Zr and Zr/Nb thin films on Si_3N_4 membranes; Design, Fabrication, Optical and Structural Characterization.

K. JIMENEZ[1,2,3,4], P. NICOLOSI[1,2], L. JUSCHKIN[3,10], NADEEM. AHMED[1,2], A.E.H. GABALLAH[1,2,5], E. CATTARUZZA[6], M. G. SERTSU[7], A. GERARDINO[8], A. GIGLIA[9], G. MUSSLER[10], P. ZUPPELLA[2].

[1]*University of Padova, Department of Information Engineering, via Gradenigo 6B, 35131 Padova, Italy.*
[2] *Italian National Research Council-Institute for Photonics and Nanotechnologies (CNR-IFN), Via Trasea 7, 35131 Padova, Italy.*
[3]*RWTH Aachen University, Experimental Physics of EUV, JARA-FIT, Steinbachstraße 15, 52074 Aachen, Germany.*
[4] *Universidad Autonoma de Santo Domingo, Santo Domingo 10105, Dominican Republic.*
[5]*National Institute for Standards (NIS), Tersa St. 12211 Giza, Egypt.*
[6]*Department of Molecular Sciences and Nanosystems, Ca' Foscari University of Venice, Via Torino 155/B, 30172 Mestre-VE, Italy.*
[7]*Institute for Nanometer Optics and Technology, Helmholtz-Zentrum Berlin (BESSY II), Albert-Einstein-Str. 15, Berlin, Germany,*
[8]*Italian National Research Council - Institute for Photonics and Nanotechnologies (CNR - IFN), Via Cineto Romano 42, Rome, 00156, Italy.*
[9]*Bear-Beamline, ELETTRA synchrotron,* SS14, Km 163.5, 34149 Basovizza TS, Italy.
[10] Peter Grünberg Institut 9 (PGI-9), Forschungszentrum Jülich GmbH, JARA-FIT, 52425 Jülich, Germany.

*kety.jimenez@gmail.com

Abstract: We investigated the optical and structural properties of Nb/Zr and Zr/Nb bilayer thin films for the development of free-standing transmittance filters in the EUV region between 5-20 nm wavelengths. Samples were deposited on Si_3N_4 membranes by magnetron sputtering technique, using metallic targets of niobium and zirconium. For better understanding of the performance of these structures and their optical and mechanical properties, single layer of Zr and Nb on Si_3N_4 membranes have also been deposited and studied. Optical microscope images show that Zr and Zr/Nb structures on membranes reveal compressive stress while Nb and Nb/Zr structures present tensile stress behavior. By etching the silicon nitride membrane, Nb and Nb/Zr self-standing filters were successfully obtained, with free-standing areas up to 3×3 mm^2 and 100 nm thickness. Transmittance performance of the samples have been measured by using EUV radiation at BEAR beamline-ELETTRA and Optics beamline-Bessy II synchrotrons. The results show the higher peak transmittance of 60% at 7.02nm and very good performance in the target range.

Keywords: EUV transmittance filters, Free Electron Laser, Freestanding filters, Nb/Zr thing films

1. Introduction:

The development and fabrication of thin film filters for extreme ultraviolet (EUV) and soft x-ray high brilliance sources are strongly required in many applications. Third and fourth generation synchrotron radiation light sources, high order harmonic generation (HHG) sources, often require extreme ultraviolet (EUV) and soft x-ray thin film filters used to remove higher-order radiation; in case of free electron laser (FEL), one of the critical technical problems is related to the rejection of high harmonics, seed laser, first stage photons (in case of two-stages FEL), and diffuse light. In order to improve the quality of the beam delivered by these sources, suitable optical systems acting as band-pass filters are necessary **[1-9]**.

The filters are also often used as gas barriers; in this case, they could interact with contaminant gases that can react with their surface causing damage or affecting their performances **[10-14]**. For these reasons the material selected for the fabrication of filters should be highly resistant, both chemically and structurally, to chemical reactions and high-power radiation. Furthermore, since materials have high absorption in the EUV and soft x-ray spectral range, filters must be very thin to achieve good transmittance performances: the selection of materials is not a trivial task.

Thin film filters are applied in other fields such as EUV lithography and spectroscopy. In space instruments development, they are used to select suitable spectral bands in order to derive plasma physical parameters through spectroscopic diagnostic techniques. **[15-18]**

FERMI is a free electron laser facility in Trieste, Italy; with two distinct branches FEL 1 and FEL 2: FEL 1 covers the spectral range 20-100 nm and FEL 2 covers the range 4-20 nm. In the case of double cascade seeded source like FEL 2 *at FERMI*, the FEL light at the selected wavelength is indeed mixed with a small fraction of the seed photons reaching the experimental chamber, with the light from the first stage and a fraction of higher harmonics. Then transmittance filters must be introduced to ensure the specific wavelength range that the experiment demands and the quality of the beam **[9, 10].** In the case of FEL, it is important that the filters have thermal and mechanical stability for high peak power radiation that is typical for such sources.

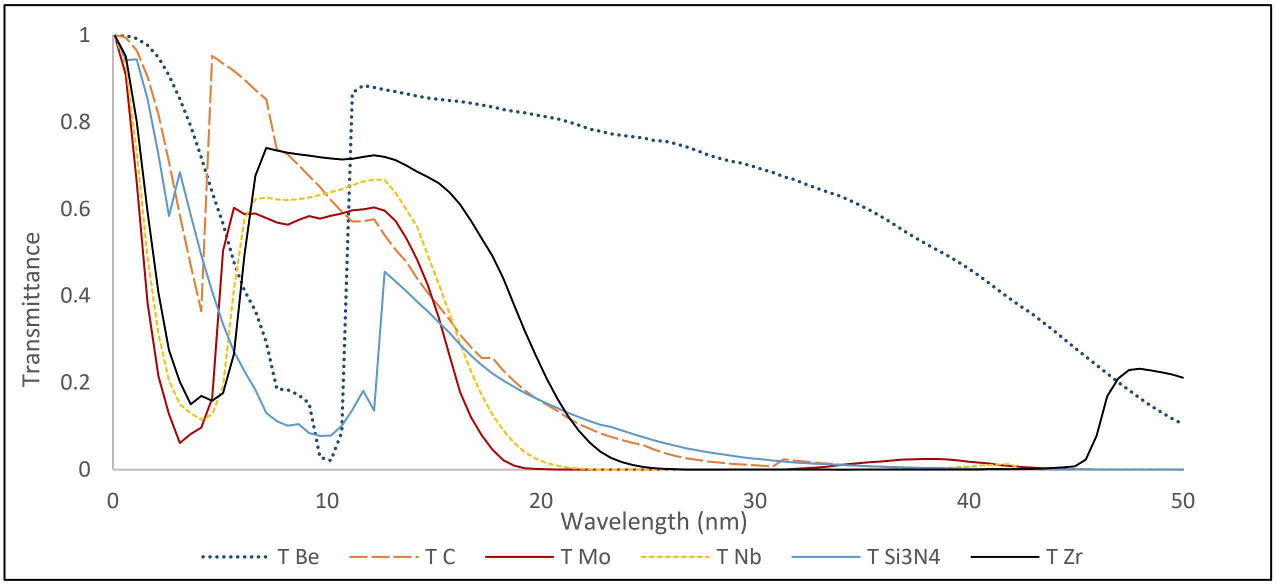

Figure 1. *Theorethical calculation of transmittance of different materials for each 100 nm thickness, in the range of 5-50 nm, using IMD software.* **[19]**

Considering their optical, chemical and mechanical properties only a few materials are good candidates for transmittance filters. In *fig 1* we can see the theoretical transmittance performance of different elements and compounds in the EUV spectral region. In this work, we are particularly interested in thin film transmittance filters for the spectral range between 4-20 nm, which is the range covered by FEL 2.

Materials such as beryllium and other rare-earth elements seem to be good candidates. But they are toxic to human health. Instead, combination of metallic-bilayers and multilayer filters have already been presented for the EUV spectral regime. Most of them are supported by metal mesh and others fabricated in free standing architectures. **[20-25].**

In this study we have chosen Zr and Nb for their relatively high transmittance in the spectral range of interest, and for their mechanical strength. Niobium belongs to the group so-called refractory metals. Refractory metals are known for their resistance to wear and to high temperatures. Nb and Zr have higher melting point and better thermal stability than other materials like Palladium or Tin, also used for thin film filters **[12, 15, 27].** Both are suited for e–beam deposition and sputtering techniques. Zr and Nb are two of the few materials with proper optical, chemical and mechanical properties for being an option for transmittance filters in the range 4-20 nm wavelength.

Single foils of Zr and Nb are being used as transmittance filters and have been tested in different wavelength ranges, for applications of extreme ultraviolet high-volume lithography instrumentation and in FELs **[12, 16, 17, 23-26],** but Zr/Nb or Nb/Zr bilayer structures have not been tested yet for any of these applications.

In 2001 Forbes R Powel and Terry A. Johnson, presented Zr films of around 100 nm supported by a Ni mesh reporting 48% of transmittance at 13.4 nm, used as filter windows for lithography application **[16]**. In 2007 V.P Belik et al. showed some results for 100 nm Nb and Zr filters supported by Si_3N_4 membranes with transmittance peak of 30% around 13nm. They also presented a 240 nm thickness Nb/Si multilayer (6 nm Nb, 6 nm Si; 20 pairs), supported by a gold mesh with 18% of transmittance near 11 nm and approximately 45% around 13 nm, as filter for nanolithography **[25].** Furthermore, Wu Heyun, also in 2007 presented self- supporting Zr filters, for soft x- ray laser applications, but with higher thicknesses 300, 400 and 500 nm; the thinnest one showing the highest, 35% peak transmittance around 13.5nm **[23].** In 2011 Yonggan Wu et al. presented Zr filters supported by a Polyamide film with 10.5% transmittance around 13 nm and 14% around 11 nm, looking for filter materials for soft x ray **[26]**. In addition, in 2011, N.I. Sckhalo et al, fabricated different multilayers structures based on Mo/$ZrSi_2$ combinations, with a transmittance peak of around 72% near 13nm, but very low transmittance for the range between 5-10nm **[24]**. In 2012 Brose S. et al. achieved free-standing Nb filters tested at 11 nm with 48% of transmittance **[17]**. C. Tarrio pursuing better mechanical structure in 2015 fabricated 250 nm Zr filters supported by a Cu mesh with a maximum peak transmittance of 48% **[12].**

In the present study, the combination of Zr and Nb in bilayer structures has been investigated to obtain filters with better mechanical properties, strong enough to achieve the fabrication of self-standing filters and high thermal stability to fulfill FEL 2 requirements. The use of a Si_3N_4 membrane as a substrate provides extra mechanical support to the samples during fabrication process. . For better understanding of the performances of these bilayer structures and their mechanical and optical properties, single layer thin films of Zr and Nb on Si_3N_4 membranes have also been deposited and studied.

Furthermore, Nb/Zr free standing filters were obtained, showing a peak transmittance of 60% at 7.02 nm, this is the best reported transmittance value until now, to our knowledge, for this wavelength.

2. Experimental: fabrication and characterization methods

Silicon nitride (Si_3N_4) membranes (from Silson Ltd) were used as substrates for the fabrication of several Zr, Nb, Nb/Zr and Zr/Nb thin film filters with different thicknesses. The membrane system structure consists of 7.5 mm X 7.5 mm silicon frame with 3 mm X 3 mm window in the center covered by the Si_3N_4 membrane. The Si_3N_4 membrane is about 100 nm thick while the silicon frame is about 200 µm thick.

Since the membranes are very fragile, custom-made holders were used to handle them during the metal evaporation and characterization of the sample, *fig 2*. Holders are made with aluminum base and copper clamps.

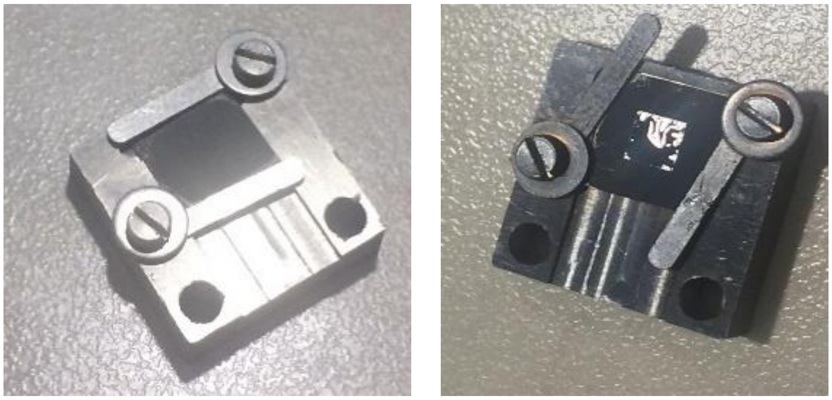

Figure 2. *Samples after deposition. Samples are mounted in custom made samples holders. 2 different kind of samples are shown, Left Nb/Zr and Zr/Nb on the right.*

In *fig 3* a schematic drawing of the fabrication process is shown. Using the mentioned substrate (step 1) we proceed with the evaporation of the metal layers on top of the substrate by using magnetron sputtering (step 2). To obtain a free self-standing filter, the Si_3N_4 substrate must be etched. Reactive ion etching (RIE) (step 4) has been applied on the membrane backside in order to open a window in the silicon nitride.

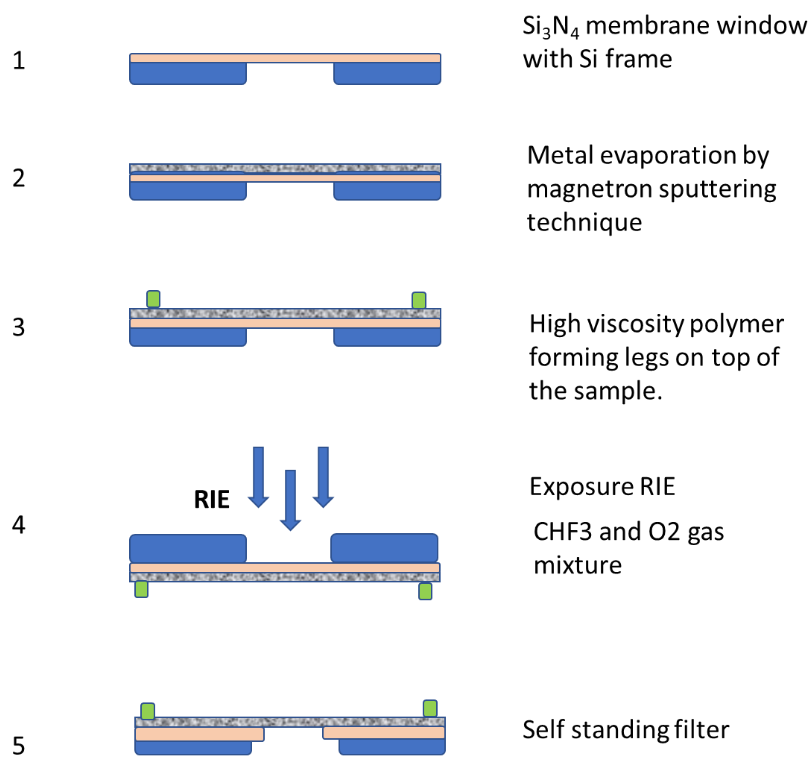

Figure 3. *Simplified fabrication process of the free self-standing filters.*

All samples were fabricated by using magnetron sputtering evaporation technique at the *Sputtering Lab of the Department of Molecular Sciences and Nanosystems, Ca' Foscari University of Venice, Italy*. Sputter depositions were performed in a custom-built radiofrequency (RF) magnetron sputtering system (13.56 MHz), equipped with three independent circular (2-inch in diameter), water-cooled, planar magnetron sources and a rf-biased sample holder. The cylindrical process chamber (equipped with a load-lock system) has both the diameter and the height equal to 60 cm, it is evacuated by the concurrent action of a turbomolecular pump and a cryogenic one. Throttle valves are placed between the pumps and the chamber to control the pumping speed. The base pressure in the chamber was in the range $1–10 \times 10^{-5}$ Pa. Depositions were performed using pure Ar (99.9995%) at a total working pressure around 50×10^{-2} Pa. The working pressure was maintained by the cryogenic pump; during the deposition, an additional and masked magnetron sputtering DC source (loaded with a pure Ti target) was also working in order to decrease the partial pressure of residual reactive gases, mainly oxygen, present in the vacuum chamber. The targets used on the two independent rf-sources were a 2-inch diameter Nb (99.95%) and Zr (99.5%) metallic disk, ¼-inch thickness. The lower purity of Zr target is mainly due to the well-known difficulty to produce Hf-free zirconium: the presence of Hf atoms in all the Zr-deposited films was confirmed by Rutherford backscattering spectrometry (RBS), showing in all films a Hf/Zr ratio of about 1%. The rf-power applied to the targets was 30 W, for time deposition ranging from 85 to 350 min. The two sources were both operated in an unbalanced-magnetron configuration. Film deposition was performed at room temperature in an off-axis configuration; the 4 inches diameter substrate holder, rotating at 10 rpm, was placed above the sources. At first, sources were conditioned for 20 min at the operating conditions to remove residual surface contaminations on the targets. To check the thickness and composition of the deposited films, additional 1×2 cm^2 flat pieces of SiO_2 (1 mm thick) have been mounted on the sample holder. A portion of the Si substrates was masked against film deposition in order to estimate the thickness of the deposited layers by measuring the step edge height with contact profiler. The deposition rate derived by profilometer measurements was subsequently checked by RBS data: for both sources, the deposition rate was of about 30 nm/h. Twelve depositions were performed, three for each kind of composition: Zr, Nb, Nb/Zr, and Zr/Nb considering 2 different thicknesses for each one; several samples were deposited at the same time, for a total of **30 samples analyzed**.

From those 30 samples fabricated and analyzed, samples with Zr and Zr/Nb structure presented compressive stress in the surface (wrinkled surface samples) while samples with Nb and Nb/Zr structures showed tensile stress (flat surface samples). We can appreciate the two different kind of stress in *fig 2 and 4*.

The composition of the synthesized layers was measured by RBS. RBS measurements were performed at *Laboratori Nazionali INFN-Legnaro (Padova, Italy)*, using a $^4He^+$ beam at the energy of 2.0 MeV, with a spot size of about 2 mm^2. The beam direction was perpendicular to the sample surface, and scattered particles were detected at the backward angle of 160◦. The used silica substrate allows an internal calibration during the data acquisition process, thus reducing the uncertainty on the amount of the detected species to lower than 5%. Depth concentration analysis of the deposited films was performed by simulating and fitting the experimental spectra using the RUMP computer code **[28].**

The surface roughness of the samples was measured in air by atomic force microscopy (AFM) using a Park System 70 XE-series AFM in non-contact mode *at CNR- Institute for Photonics and Nanotechnologies IFN (CNR-IFN) Padova, Italy*. The scanned area was 5x5 μm^2. The root-mean-square (RMS) and average surface roughness (Ra) were determined by using XEI data analysis software (Park Systems Corp). Measurements were taken for the substrate and for the deposited samples. The silicon nitride membranes used as substrates show always roughness values less than 1.6 nm.

Three months after the deposition, the transmittance of one of the samples based on **Nb/Zr** was characterized at the *Optics Beamline at **BESSY II** synchrotron, Berlin, Germany* **[29]**. The transmittance measurements of the rest of the samples were carried on **one year after deposition** at the *BEAR beamline of ELETTRA – Synchrotron, Trieste, Italy.* Samples were storage, mounted each one in a custom-made holder, in Polypropylene (PP) boxes of the similar size to avoid movement of the sample during transportation.

The Optics beamline at BESSY II, is a soft x-ray bending magnet beamline equipped with plane grating monochromator, operated in collimated light. It is optimized to offer good resolution at very high spectral purity and efficient stray light reduction by a 4-mirror high order suppressor (HIOS) and a filter and slit units (FSU). A permanent end-station, located in a clean-room hutch, possesses inside a versatile reflectometer for at-wavelength metrology, covering spectral range from 10-2000 eV **[30].**

BEAR is a bending magnet beamline dedicated, among others, to reflectance and transmittance measurements **[31-32].** It covers an energy band from visible light to 1.6 keV, delivering radiation with well-defined spectral purity properties. The sample chamber is equipped with motors enabling movements of the sample holder in all directions (six degrees of freedom), accurate alignment, and scans in a vast angular range. Finally, a sample insertion chamber with locking transfer system allows to change and insert samples without venting.

Some of the samples were treated by etching procedure to separate the metal thin films from the Si_3N_4 substrate. The treatment was performed at *CNR - IFN UOS Rome*, *Italy*. A reactive ion etching (RIE) of Si_3N_4 membrane was carried on the back side of the sample by using a gas mixture of CHF_3 and O_2 plasma. The samples were inserted in the RIE chamber with the backside upward in order to better expose the membrane to the etching plasma, protecting the front side from damage or contamination of the film surface. We used the following recipe: 50 sccm CHF_3, 10 sccm O_2, RF power: 175 W, pressure: 55 mTorr, V bias: 250V; different samples were etched in order to adjust the etching time. Due to the lower mechanical stability of the wrinkled samples (Zr, and Zr/Nb structures), etching was unsuccessful, samples were fragile, getting broken during RIE exposure. In contrast flat samples (Nb, Nb/Zr) were mechanically stable for the etching process. The membrane was successfully removed after an exposure time of 4 minutes, resulting in free-standing Nb, and Nb/Zr filters, of this two, we will focus on Nb/Zr type because has shown better performance.

To get more information about the structure of Nb/Zr free standing filter, X-ray diffraction (XRD) measurements were accomplished by using a high-resolution Bruker D8 diffractometer, Cu_K_alpha = 0.15406 nm, employing a scintillator detector with a mechanical slit of 3 mm. The equipment is located in Peter Gruenberg Institute-9 facilities at the Forschungszentrum Jülich. The scans were carried out in a range from 2Theta = 3° – 140° with angular resolutions of 0.1°. Each data point was measured for 10s.

Scanning electron microscopy (SEM) was also applied to investigate the properties of the free-standing sample. The measurements were performed at the imaging facilities of HFN Jülich, using a FE-SEM ZEISS SIGMA 300 (field emission scanning electron microscope), at the accelerating voltage of 20 kV.

Also, XPS measurements were performed on the sample by using the Phi5000 VersaProbe II, ULVAC-Phi Inc., USA. The instrument is operated at Al K-alpha, with a monochromatic source of 1.486 keV. The measurements were carried on three 200µm size spots, with 187.5 eV pass energy, 0.8 eV step, and 100ms/step. The results are presented with quantification in atomic percentage (at%) and 15% relative error, normalized to 100 at%, with a Shirley background and empirical relative sensitivity factors. The instrument is located at the Central Institute for Engineering, Electronics and Analytics (ZEA-3) at Forschungszentrum Jülich.

We have selected **seven** of the 30 samples to resume the results of the different types of material combinations. The description of the samples and the measurements performed on each one of them are presented in *Table 1*.

Table 1. *Description of the samples used for the resume of the results of the research and measurements performed on them.*

Samples	**Substrate (100nm)**	**Nominal thicknesses of individual layers (nm)**	**Total thickness of metal layer (nm)**		**Measurements performed**				
				RBS	**AFM Roughness**	**Transmittance**		**XRD**	**XPS**
						At BESSY II 3 months after deposition	**BEAR 1 year after deposition**		
Nb	Si_3N_4	100	104	*	*		*		
Zr_1	Si_3N_4	100	108	*	*				
Zr_2	Si_3N_4	150	169	*			*		
Zr/Nb	Si_3N_4	50/50	103	*	*		*		
Nb/Zr_1	Si_3N_4	50/50	107	*	*	*			
Nb/Zr_2	Si_3N_4	50/50	107	*			*		
Nb/Zr_3	Etched (no -substrate)	50/50	107	*			*	*	*

3. Results and discussion

After deposition, the samples were characterized by RBS in order to detect contaminants due to the fabrication process and raw materials impurities. The specimens mostly show oxygen contamination. The oxygen concentration is not uniform with depth: in some samples oxygen probably diffused from the outside due to the air exposure, in other cases a relatively large presence of oxygen at the interface substrate/film could suggest a gettering effect at the start of the deposition.

Table 2 reports a summary of the RBS results: for each sample, the mean stoichiometry of the different layers was calculated. Since the density of the different detected compounds is unknown, the reported layer thickness was retrieved by assuming a hypothetical pure metal layer, the bulk metal density and the detected amount of metal. Samples Nb/Zr_1, Nb/Zr_2 and Nb/Zr_3 were deposited together, then we are assuming the three samples have the same chemical composition. The oxygen contamination mainly affects the Zr_1, Zr_2 and Zr/Nb films.

Both Zr and Nb oxidize readily when they are exposed to air. Zr oxidize at faster rate than Nb as it shows in table 2. From literature we know that the most common oxidation state of Zr, in thin metallic films, is ZrO_2, while for Nb is Nb_2O_5. The material's density changes with oxidation, producing the expansion of the layers thicknesses, resulting in the appearance of some intrinsic stress in the film. The lower rate of oxidation and possible plastic deformation of Nb layers could allow the relieve of the residual stress. **[27,33,34,35]**

Table 2. Mean stoichiometry of the different deposited layers calculated from RBS data. Thickness* is related to a hypothetical pure metal layer containing the detected amount of metal.

Sample	**Nominal total thickness (nm)**	**Top layer (mean composition − thickness*)**	**Bottom layer (mean composition − thickness*)**
Nb	100	$NbO_{0.3}$ − 104 nm	–
Zr _1	100	$ZrO_{1.1}Hf_{0.01}$ – 108 nm	–
Zr_2	150	$ZrO_{0.1}Hf_{0.01}$ − 169 nm	--
Zr/Nb	100	$ZrOHf_{0.01}$ – 49 nm	$NbO_{0.2}$ − 54 nm
Nb/Zr (1,2,3)	100	$NbO_{0.1}$ − 50 nm	$ZrO_{0.4}Hf_{0.01}$ – 57 nm

Also, the strain strongly depends on the selected top layer. *Fig.4* depicts examples of filters grown with compressive and tensile strain. The top images of figure 4 refer to Nb and Nb/Zr_1 samples, with Nb on the top. In this case, a smooth homogenous structure with tensile stress is observed. The bottom images show Zr_1 and Zr/Nb specimens: the surface is wrinkled by compressive stress.

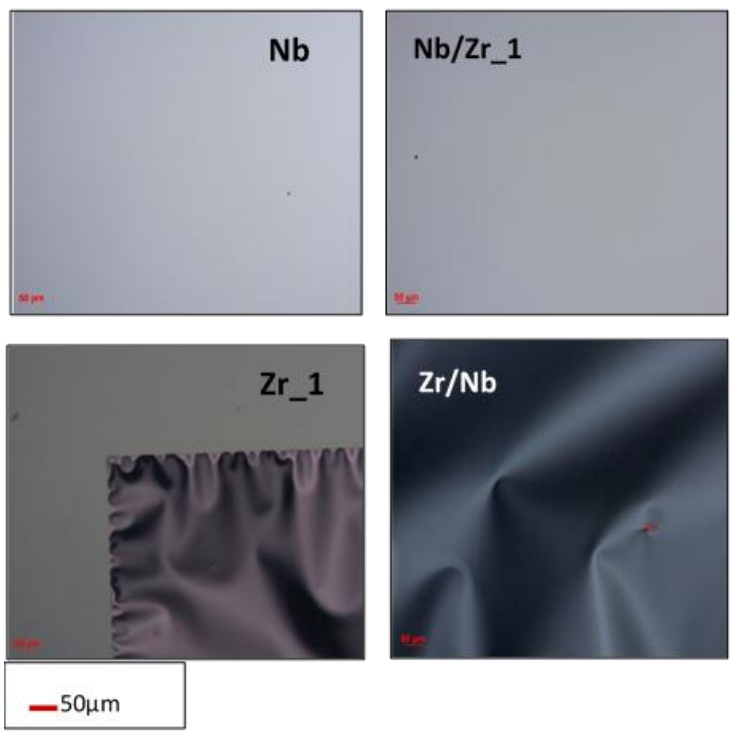

Figure 41. *Optical images of the surfaces on the different material samples on Si_3N_4. Nb and Nb/Zr, flat samples, grown with tensile stress, (top images). Zr and Zr/Nb, wrinkled samples, grown with compressive stress, (bottom Images).*

Regarding the nanoscale observation, the surface roughness of the Nb and Nb/Zr samples is almost the same as that of the substrate, while in case of Zr and Zr/Nb structures the surface experiences an increase of roughness, particularly in the Zr specimen. The results of the morphology analysis performed by AFM are summarized in table 3:

Table 3. *Summary of surface roughness values measured by AFM*

Sample	Nominal thickness (nm)	Roughness (nm)
Si_3N_4(substrate)	100	1.4±0.2
Zr_	100	3.4±0.2
Nb	100	1.4±0.1
Zr/Nb	100	1.8±0.2
Nb/Zr_	100	1.4±0.1

The roughness and the stress of the films can affect the properties of the wavefront passing the filter, by inducing distortion of the incoming beam, also can affect the quality of the films and the mechanical stability of the filters. Furthermore, Zr and Zr/Nb samples exhibiting high surface roughness and compressive stress are not the best candidates for etching process. In fact, we know that they didn't survive the etching.

The filters with the tensile strain (Nb and Nb/Zr_1), on the contrary, demonstrate a flat surface, suitable for achieving a successful etching process and for the filters manufacturing. The reduction of the compressive stress is due to the presence of Nb as top layer. The stress in Zr thin films could be related to the pronounced oxidation of Zr during deposition and the continuing escalated oxidization due to exposure with the air, after deposition. **[33-34]**

Fig. 5 shows the optical microscope images of the Nb/Zr filter surface structure before and after the etching procedure. Due to the detachment of the silicon nitrate membrane, we can observe how the membrane releasing changes the stress on the surface of the sample.

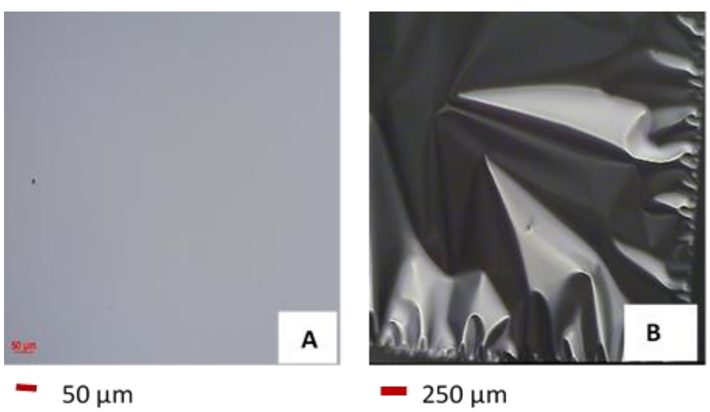

Figure 5. *Optical microscope images of the Nb/Zr sample before etching procedure (left) and after etching procedure (right).*

Transmission measurements were performed before the etching for the samples of interest in the EUV region 40-410 eV (3-31 nm) with steps of 0.2 eV.

In *fig 6* we present the results of transmittance measurements for Nb/Zr_1 (BESSY II) and Nb/Zr_2 (BEAR) samples. As mentioned before, they were deposited together in the same chamber; sample Nb/Zr_1 was measured 3 months after deposition while sample Nb/Zr_2 was measured 1 year after deposition in order to evaluate possible effects of aging and contamination on the transmittance performance of the filters.

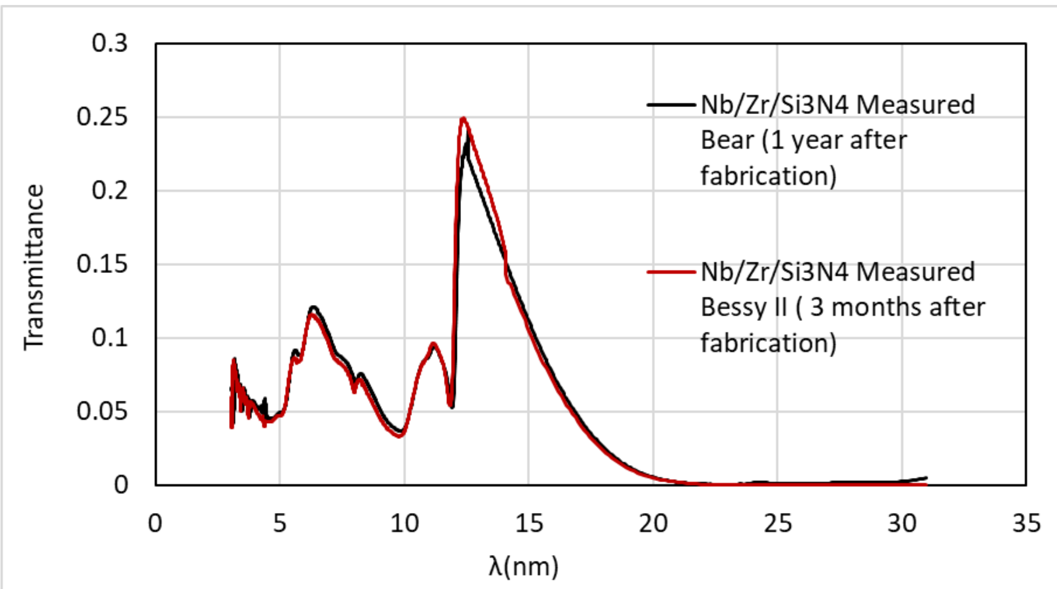

Figure 6. *Measured transmittance comparison between sample Nb/Zr_1 and Nb/Zr_2. Samples were fabricated together, in the same chamber; they have the same thicknesses. Transmittance of Nb/Zr_1 was measured 3 months after and Nb/Zr_2 was measured 1 year after fabrication.*

There is a minimal difference in the transmittance spectra of the two samples between 3-31nm. Since the samples characterized are not exactly the same, we cannot directly conclude that the slight reduction of performance is due to the aging. However, taking in account that the samples were fabricated during the same deposition run and were kept in similar packing conditions, the results are a good indication of the chemical stability and wear resistance of Nb/Zr bilayer.

After one year, also the samples Zr_1, Nb, and Zr/Nb were characterized in terms of transmittance at BEAR beamline. The total thickness of the metal layers for all the samples is around 100 nm plus 100 nm of the Si_3N_4 membrane. The idea was to compare structural and optical performance of them. The 100 nm Zr sample appears more fragile than Nb one and bilayers. This is possibly due to the higher compressive stress that it showed after deposition. During handling and measurement, the 100 nm Zr samples got broken. Then, we decided to use a thicker sample of around 169 nm of Zr (Zr_2) to study the properties of single layer Zr.

Fig 7 shows the experimental transmittance of the measured samples together with the transmittance curves obtained by IMD simulation; using theoretical optical constants of the targeted materials assuming the RBS thickness results and no contamination. All the samples exhibit lower transmittance compared to the calculated data (the Si_3N_4 membrane was considered in the simulated curves). The reduction of transmission could have two possible causes:

1. different level of oxidation in the surface and through the sample as RBS results showed;
2. different kind of contamination on the surface and oxidation of the sample.

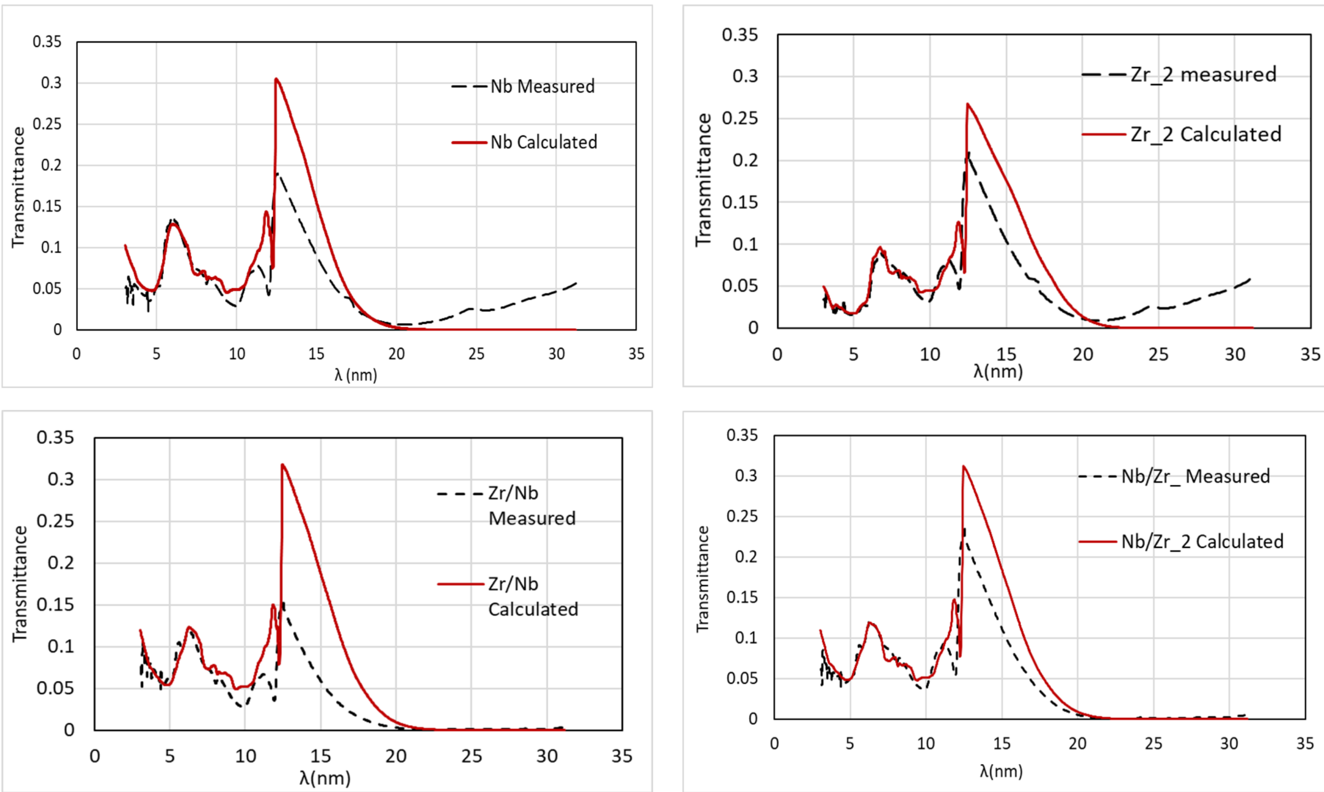

Figure 2. *Transmittance curves of the samples deposited on Si_3N_4 membrane substrates, (not etched samples). The graphs show the comparison between the calculated and the measured values of transmittances for the different samples*.

Fig 8 shows the comparison between four of the measured samples and the theoretical transmittance of the silicon nitride membrane. As we can observe, Nb/Zr_2 exhibits the higher peak transmission, approximately 24% around 12.55 nm. Zr/Nb sample, on the contrary, shows lower transmittance performance. The 100 nm Zr specimen theoretically should have better transmittance performance, but it didn't survive the measurement campaign and we don't have any experimental results for it. Some studies have linked the compressive stress in sputtered zirconium thin films to the low pressure during the deposition, and to the transition from metallic to oxidized film **[33-34]**. As it was shown before, in *Table 2*, higher concentration of oxygen was present in Zr/Nb specimens. This could mean an increase of oxidation of the sample, which explains the lower transmittance response.

For the same thickness, the stiffness of the Nb guarantees stable structures on membrane **[17]**, but with lower transmittance performance than Zr. In fact, the transmission of the Nb is slightly below of the widely used zirconium filters and below of the Nb/Zr free standing filter, proposed in this manuscript (see *fig 7*). The bilayer structure of Nb/Zr combines the higher mechanical stability of Nb with the higher transmittance performance of Zr in this specific spectral region, resulting in the best candidate for free-standing filters.

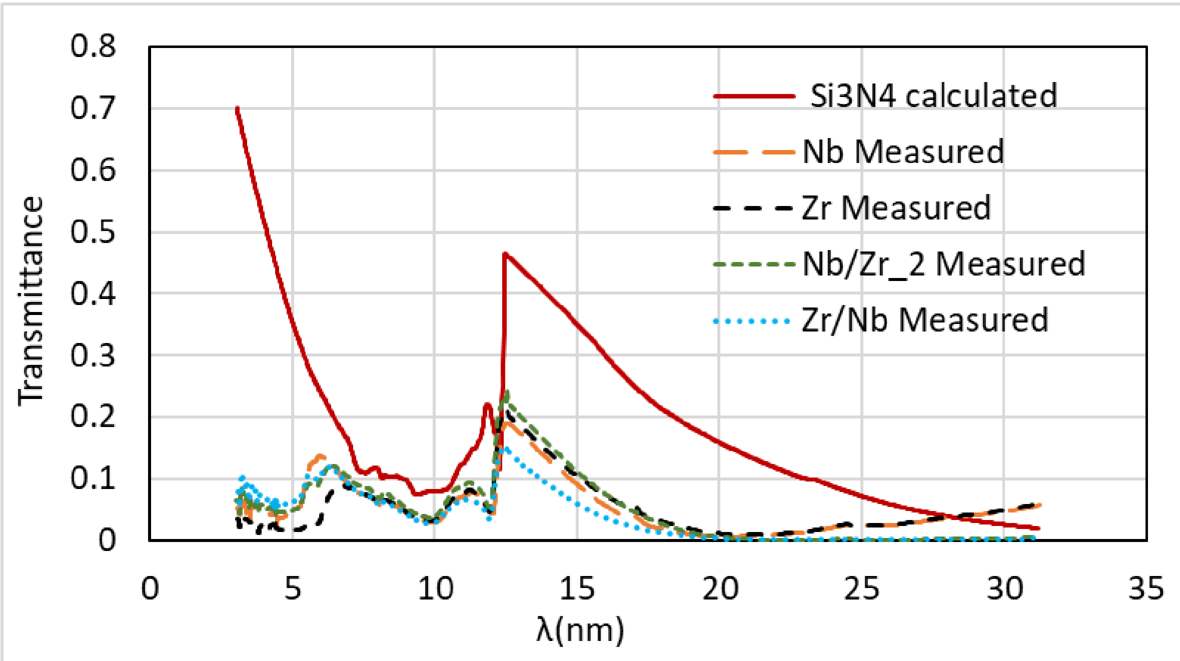

Figure 83. *Comparison of the transmittance values of all the samples and the calculated values of transmittance for the Si3N4 membrane substrate*.

The etching process was tried out on the four different types of samples, and as it was mentioned before, only Nb and Nb/Zr samples survived the etching process proving to have high mechanical stability.

In this section we mainly focus on the new free-standing Nb/Zr filter which, based on simulated data, could offer higher transmittance performance than monolayer Nb of the same thickness. Sample Nb/Zr_3 (see table 1) corresponds to the Nb/Zr free standing filter (etched sample). We did not test Nb free-standing filter.

We performed XRD measurements of this sample. Besides the Si substrate peaks, signatures of the Nb/Zr epilayers were found. These peaks are attributed to the Zr in the hcp crystal structure at 32.2° and Nb in the bcc lattice configuration at 38.0°, as it is shown in *fig 9*.

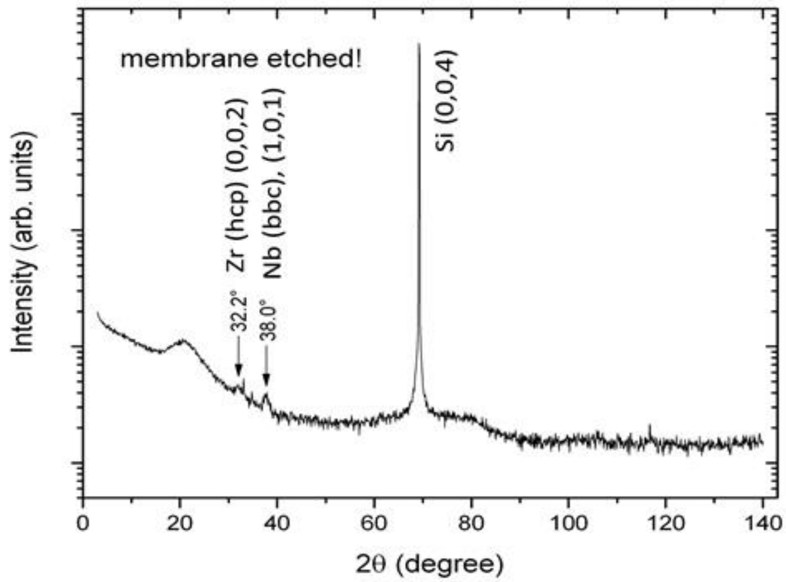

Figure 4. *XRD measurements. Signatures of Niobium and Zirconium were found, and also the signature of Silicon due to the frame of the samples.*

Due to the polycrystalline nature of the sample's structures, the picks are not strongly sharp, however well identifiable SEM images depict (*fig. 10*) the surface of the Nb/Zr_3. In the left image, filter window area and silicon frame can be distinguished; in the right, the polycrystalline structure is observed.

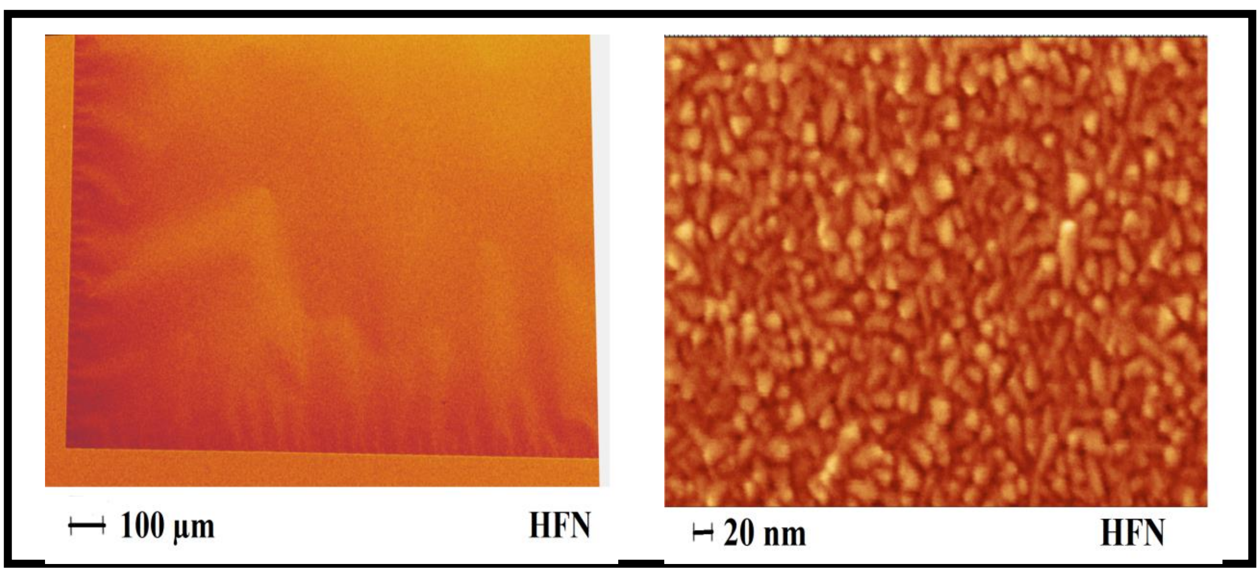

Figure 5. *SEM images of Nb/Zr_3 (free self-standing filter) around 100 nm thickness. In the left image, it could be appreciated how the tensile stress was released. In the right, image of the surface nanostructure is shown.*

The transmittance of Nb/Zr free standing filter was measured at BEAR beamline between 40-420 eV (3-31 nm).

A rough transmittance scan was performed on the sample along horizontal (Y-axis) and vertical (Z axis), using 40 eV photon energy for studying the uniformity of the filter. Results are presented in *fig. 11*. The membrane window is about 3 mm x 3 mm. The signal is very stable inside the window area along both axes, demonstrating a uniform bilayer structure.

Subsequently, the transmittance was measured in the complete wavelength range. The results are in *fig. 12*. The difference in transmittance before and after the etching procedure is shown in *fig 12 left*. A considerable increase of transmittance is notable as it is expected after the membrane is removed. The filter possesses the higher transmittance's peak at 7.02 nm of about 60%. At 11nm the transmittance is 47.5% a little bit lower than the results presented by Brose S. et all in 2012, but higher than for filters proposed by other authors **[12, 25, 26]**. Brose measured a Nb free standing filter with 48% of transparency at 11 nm **[17]**. We present broad-band characterization of the high throughput Nb/Zr free standing filter developed in this work and thought for a wide wavelength range.

Fig 12 right shows the comparison between theoretical transmission curves and measured one of the investigated filter. We present two theoretical curves: "Nb/Zr Calculated 1" corresponds to the IMD simulated transmission for 107 nm ideal Nb/Zr filter by ignoring any contamination or oxidation of the materials. As we can observe, the measured and Calculated 1 curve have big discrepancies, then we simulated the transmission of a more realistic structure. In "Calculated 2" curve, we considered the RBS thicknesses results, we simulated the Nb/Zr filter assuming a thin layer of Nb_2O_5, most common oxidation state for Nb thin film **[35-36]**, on top of the Nb layer and a thin layer of ZrO_2 at the interface **[27, 33, 34]**.

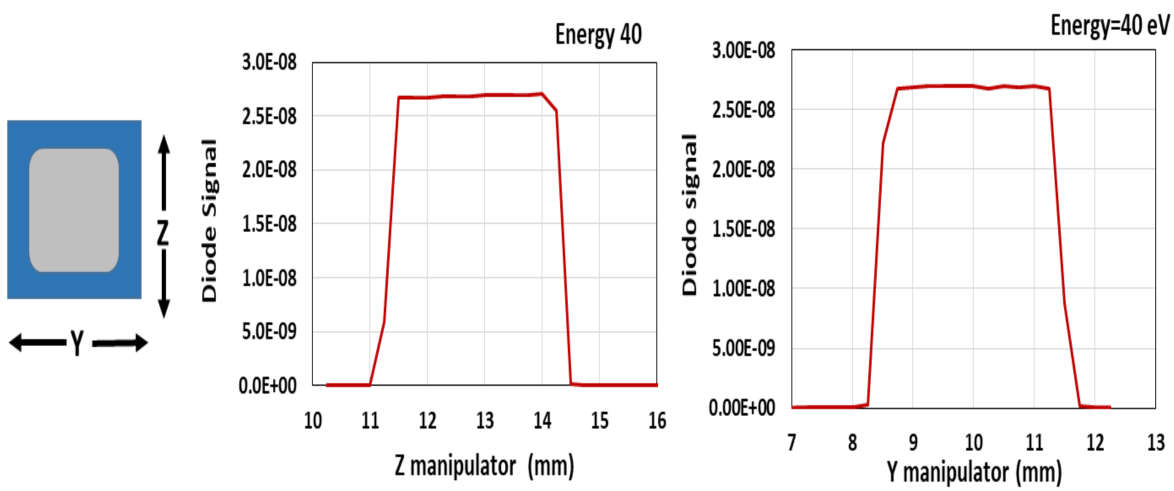

***Figure 6**. Y and Z Scan of the sample using an energy of 40 eV to study uniformity of the sample. The filter window is about 3mm x 3mm, and the transmitted signal looks very stable.*

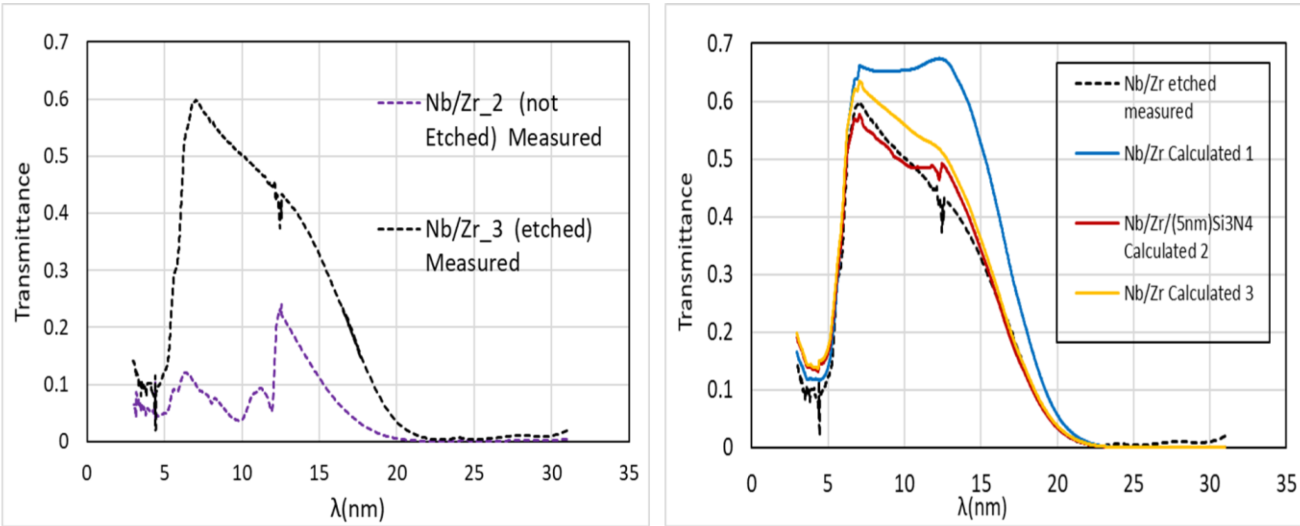

Figure 7. *Left. Comparison of transmittance values of Nb/Zr (Nb/Zr_2) before and after the etching process (Nb/Zr_3). Right. Comparison of transmittance measured values of Nb/Zr free standing filter (Nb/Zr_3) in contrast with the IMD simulated transmittance considering only the nominal thickness of the sample in the Calculated 1 curve. Calculated 2 curve is simulated considering the nominal thickness, layers of oxidation of the materials, carbon contamination and 5 nm of a residual Si_3N_4 membrane. Calculated 3 curve is simulated using the same structure of Calculated 2 but assuming complete etching (no residual membrane).*

Furthermore, since Carbon is as a common type of contamination on metal filters exposed to the environment, we added in the simulation 4 nm of carbon on the surface. In the model, a 5 nm thin layer of Si_3N_4 has been also added to the bottom of the structure to take into account the possible residuals of the membrane after the etching process. The final structure (*fig. 13*) used for the simulation of the Calculated 2 Curve is the following, from top to bottom:

1) C layer = 4.00 nm
2) Nb2O5 layer = 7.00 nm
3) Nb layer = 42.00 nm
4) ZrO2 layer = 20.00 nm
5) Zr layer = 37.00 nm
6) Si3N4 layer = 5.00 nm
7) C layer = 5.00 nm

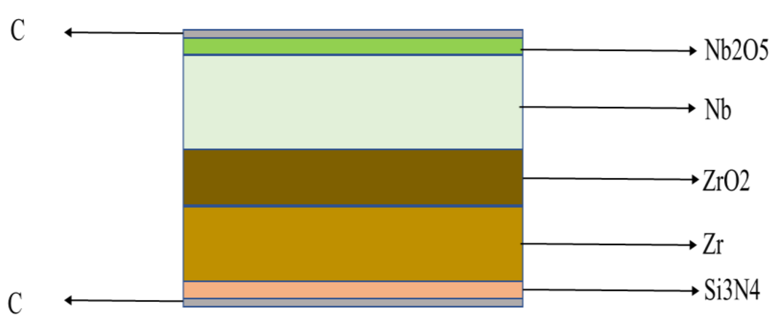

Figure 13*. Filter Structure used for obtaining the transmittance simulated curve Calculated 2, which agreed more closely to the measured curve.*

Indeed, the measured and Calculated 2 curves are very similar. We can deduce that our hypotheses of contamination have some grounds. In Calculated 3 curve, we consider the same carbon and oxygen contamination as in Calculated 2, but in this case, we are assuming a completed etching (no presence of residual membrane). The transmittance of the filter is improved in case of achieving complete etching. Furthermore, we can conclude that carbon contamination and oxidation of the metal layers are the higher contributors to the reduction of the transmittance performance of the filter. Some absorption features can be found in the measured data at 4.39 nm and 4.45nm corresponding to Carbon K absorption edge and at 12.2 nm and 12.4 nm, where the LII and LIII Silicon absorption edges are present. These lines are found not only in the experimental analysis, but also in the Calculated 2 curve.

To test the hypotheses of surface contamination other than the initial oxidation levels found in the RBS results after the fabrication of the samples, XPS mapping in three different spots of the free-standing filter was performed. *Fig 14* shows the image of the three spots randomly selected to determine the homogeneity (about 8nm deep) of the contamination at the sample surface.

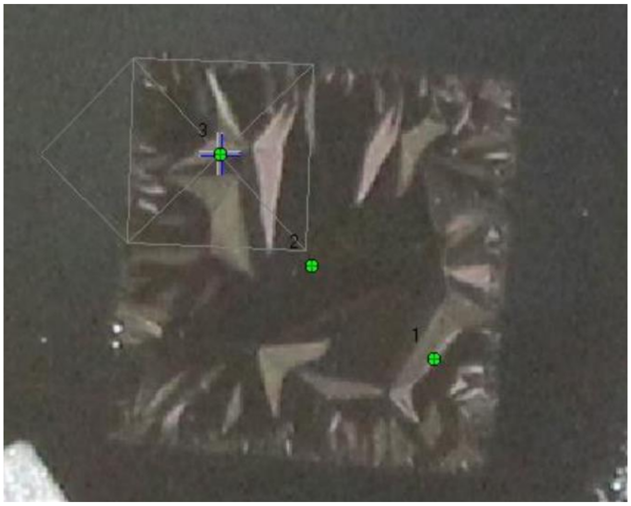

Figure 14. *XPS analysis was performed in the 3 different shown spots.*

In *fig 15* the XPS spectrum from one of the spots is reported and in *table 4* results from the survey of the three spots are displayed.

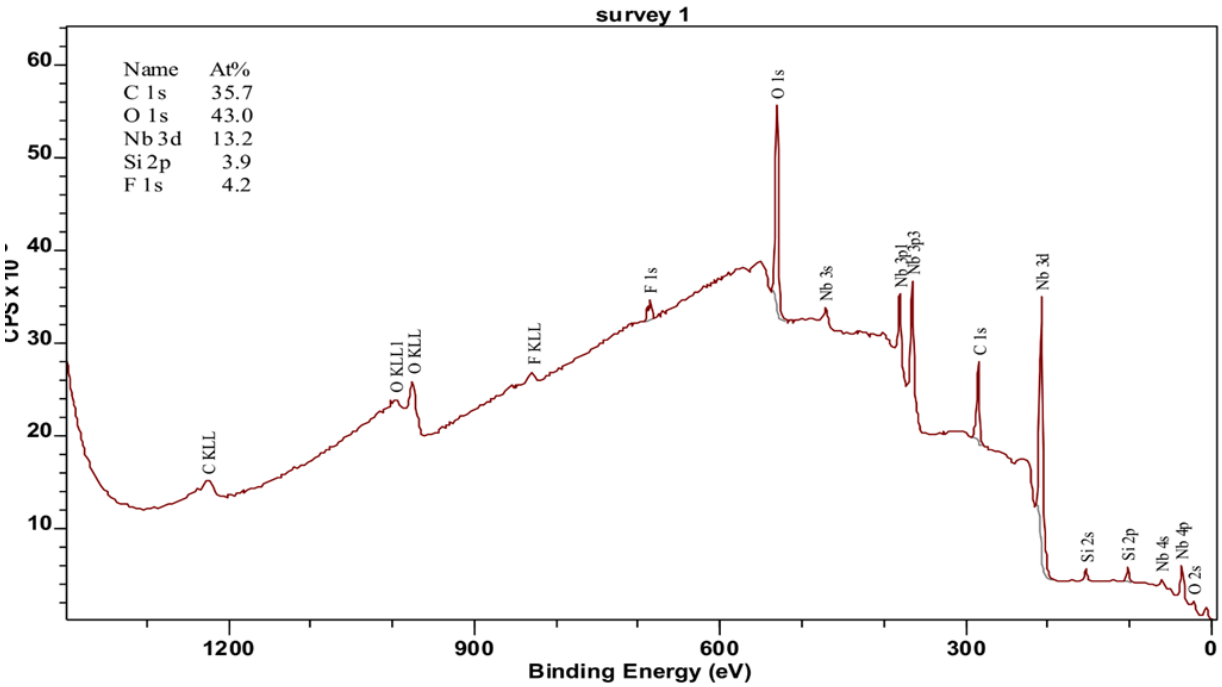

Figure 15. *XPS spectrum of one spot measured on the Nb/Zr free standing filter.*

Table 4. *Quantification in at% of elements found on the surface of the free-standing filter. The analysis can reach between 5 to 8 nm deep.*

Elements found	**Spot 1 (At %)**	**Spot 2 (At %)**	**Spot 3 (At%)**
C	35.7	35.0	37.0
O	43.0	42.3	41.3
Nb	13.2	13.1	12.4
Si	3.9	4.7	4.5
F	4.2	4.9	4.8

The results indicate the presence of carbon contamination on the surface on top of a natural oxide layer of Nb_xO_x. Furthermore, some Si and F traces were found on the surface. The XPS results agree with the transmittance performance of the filter as we have shown in Calculate 3 curve.

Conclusions:

Nb and Zr, have good transmittance performance between 5-20 nm, they are good candidates for EUV filters for FEL 2 at FERMI that cover specifically this range. The transmission of the Nb is slightly lower than that of widely used zirconium filters, but the higher stiffness of the Nb allows obtaining more stable filters of the same thickness. The use of the combination of these two materials, in bilayer structures, brings together the good transmittance performance of Zr and the stiffness of Nb which makes Nb/Zr an excellent choice for fabrication of thinner free standing EUV filters.

Nb/Zr free standing filters were obtained, showing a peak transmittance of 60% at 7.02 nm, this is the best reported transmittance value until now, to our knowledge, for this wavelength. In the case of the filters on Si_3N_4 membranes the maximum transmittance achieved was approximately 24% around 12.55 nm. Due to the high compressive stress of Zr and Zr/Nb on Si_3N_4 samples, etching the membrane was not possible. On the other hand, for the samples that showed flat, tensile stress surface, the etching process was successful, obtaining free self-standing Nb, Nb/Zr filters. Besides the presence of a residual thin layer of Si_3N_4 at the bottom of the sample, the XPS analysis of the Nb/Zr free standing filter indicated that the reduction of the expected values of transmittance could be due to the surface contamination and some level of oxidation of the metal layers. It is recommended to grow an oxidation protection layer in situ with the metal material deposition to avoid progressive oxidation of the filters.

Acknowledgments.

This project research is supported by the Education, Audiovisual and Culture Executive Agency (EACEA) Erasmus Mundus Joint Doctorate, Project No.2012 – 0033. The first author is part of the EXTATIC Program. We would like to acknowledge the excellent collaboration of the HNF cleanroom staff, and to the colleagues of PGI9 group and its Director Prof. Detlev Grützmacher; Also, to Mr. Heinrich Hartmann from ZEA3 group and our colleagues at the Forschungszentrum Jülich. Special gratitude to Prof. S. Nannorone, Prof. Luca Pasquali and PhD Kostantin Koshmak from Bear beamline at ELETTRA Synchrotron, where we had one proposal accepted. and to Frank Schaefer and Andrey Sokolov from Optics Beanline at Bessy Synchrotron. Thanks to dr. G. Maggioni (University of Padova, Physics and Astronomy Department) for RBS data acquisition at Laboratori Nazionali INFN-Legnaro, Italy).

References:

[1] Masatoshi Hatayama et al. High-Transmittance Free-Standing Aluminum Extreme Ultraviolet Filter. *Jpn. J. Appl. Phys.* **48** 122202. (2009).

[2] Gann E; Young AT; Collins BA; Yan H, Nasiatka J; Padmore HA; Ade H; Hexemer A; Wang C. "Soft x-ray scattering facility at the Advanced Light Source with real-time data processing and analysis". Review of Scientific Instruments 83, 045110 (2012).

[3] Y. Saitoh, H. Kimura; Y. Suzuki; T. Nakatani; T. Matsushita; T. Muro; T. Miyahara; M. Fujisawa; K. Soda; S. Ueda; H. Harada; M. Kotsugi; A. Sekiyama; S. Suga. "Performance of a very high-resolution soft x-ray beamline BL25SU with a twin-helical undulator at SPring-8". Review of Scientific Instruments 71, 3254 (2000).

[4] Wayne R. McKinney; Dmitri Mossessian. "Efficiency and stray light measurements and calculations of diffraction gratings for the Advanced Light Source". Review of Scientific Instruments 66, 2160 (1995).

[5] J.H Underwood; E.M Gullikson, “High-resolution, high flux, user friendly VLS beamline at the ALS for the 50– 1300 eV energy region”, Journal of Electron Spectroscopy and Related Phenomena 92, 265–272. (1998).

[6] F Bencivenga; S Baroni; C Carbone; M Chergui; M B Danailov; G De Ninno; M Kiskinova; L Raimondi; C Svetina; C Masciovecchio. “Nanoscale dynamics by short-wavelength four wave mixing experiments”. New Journal of Physics 15 (2013).

[7] O'shea P.G.; Freud H.P. Free-electron lasers: status and applications. Science 292, 1853, (2001).

[8] M. G. Pelizzo; A. J. Corso; G. Monaco; P. Nicolosi; M. Suman; P. Zuppella; D. Cocco. “Multilayer optics to be used as FEL fundamental suppressors for harmonics selection”. Nuclear Instruments and Methods in Physics Research Section A: Accelerators, Spectrometers, Detectors and Associated Equipment, ISSN: 0168-9002, Vol: 635, Issue: 1, Page: S24-S29, (2011).

[9] A. J. Corso; P. Zuppella; P. Nicolosi; D. Cocco; M. G. Pelizzo. “Multilayer mirrors for FERMI at ELETTRA beam transport system”. Proceedings Volume 8078, Advances in X-ray Free-Electron Lasers: Radiation Schemes, X-ray Optics, and Instrumentation; 80780F (2011) https://doi.org/10.1117/12.886870.

[10] C.J. Bocchetta et al. FERMI@Elettra Conceptual Design Report. Technical Report ST/F-TN-07/12, Sincrotrone Trieste. (2007).

[11] M. Zangrando; D. Cocco; C. Fava; S. Gerusina; R. Gobessi; N. Mahne; E. Mazzucco; L. Raimondi; L. Rumiz; C. Svetina. “Recent results of PADReS, the Photon Analysis Delivery and Reduction System, from the FERMI FEL commissioning and user operations”. J. Synchrotron Rad. 22, 565-570, (2015).

[12] Tarrio, C.; Berg, R. F.; Lucatorto, T. B.; Lairson, B.; Lopez, H.; Ayers, T. “Thermally stable thin-film filters for high-power extreme-ultraviolet applications”, The Review of Scientific Instruments, 86(11), 116103. (2015).

[13] Powell, F. R. 'Care and Feeding of Soft X-Ray and Extreme Ultraviolet Filters', Laser-Induced Damage in Optical Materials: SPIE Proc. 1848, 503, (1992).

[14] S. B. Hill; N. S. Faradzhev; L. J. Richter; S. Grantham; C. Tarrio; T. B. Lucatorto; S. Yulin; M. Schürmann; V. Nesterenko; T. Feigl; "Optics contamination studies in support of high-throughput EUV lithography tools, " Proc. SPIE 7969, Extreme Ultraviolet (EUV) Lithography II, 79690M. (25 March 2011).

[15] H.A. Macleod: Thin-film Optical Filters, Institute of Physics Publishing, Bristol and Philadelphia, (2001).

[16] Forbes R. Powell; Terry A. Johnson, "Filter windows for EUV lithography", Proc. SPIE 4343, Emerging Lithographic Technologies V, (20 August 2001).

[17] Brose S.; Danylyuk S.; Juschkin L.; Dittberner C.; Bergmann K.; Moers J.; Panaitov G.; (...), Grutzmacher D.; Broadband transmission masks, gratings and filters for extreme ultraviolet and soft X-ray lithography. Thin Solid Films, 520 (15), pp. 5080-5085. (2012).

[18] Slemzin, V.A.; Goryaev, F.F; Kuzin, S.V. Spectroscopic diagnostics of the solar coronal plasma. Plasma Phys. Rep. 40: 855. (2014).

[19] IMD - Software for modeling the optical properties of multilayer films, D. L. Windt, Computers in Physics, 12, 360 (1998).

[20] N. I. Chkhalo; M. N. Drozdov; E. B. Kluenkov; S. V. Kuzin; A. Ya. Lopatin; V. I. Luchin; N. N. Salashchenko; N. N. Tsybin; S. Yu. Zuev, "Thin film multilayer filters for solar EUV telescopes," Appl. Opt. 55, 4683-4690, (2016).

[21] Terry A. Johnson; Regina Soufli; Eric M. Gullikson; Miles Clift. "Zirconium and niobium transmission data at wavelengths from 11-16 nm and 200-1200 nm", Proc. SPIE 5538, Optical Constants of Materials for UV to X-Ray Wavelengths, (14 October 2004).

[22] David L. Windt; Webster C. Cash; M. Scott; P. Arendt; B. Newnam; R. F. Fisher; A. B. Swartzlander. "Optical constants for thin films of Ti, Zr, Nb, Mo, Ru, Rh, Pd, Ag, Hf, Ta, W, Re, Ir, Os, Pt, and Au from 24 Å to 1216 Å, ". Appl. Opt. 27, 246-278. (1988).

[23] Y. Wu; L. Zhang; H. Cao; X. Zheng; H. Jiao; and L. Chen. "Preparation and Characterization of Free-Standing Zr Filter for Soft X-ray Laser Application," in Optical Interference Coatings, OSA Technical Digest (CD) (Optical Society of America, 2007).

[24] N. I. Chkhalo; M. N. Drozdov; S. A. Gusev; E. B. Kluenkov; A. Ya. Lopatin; V. I. Luchin; N. N. Salashchenko; L. A. Shmaenok; N. N. Tsybin; B. A. Volodin. "Freestanding multilayer films for application as phase retarders and spectral purity filters in the soft x-ray and EUV ranges", Proc. SPIE 8076, EUV and X-Ray Optics: Synergy between Laboratory and Space II, 80760O (4 May 2011).

[25] Belik, V.P.; Zadiranov, Y.M.; Il'inskaya N.D. et al. Free-standing optical filters for a nanolithography source operating in the 12–15 nm wavelength range. Tech. Phys. Lett. 33: 508, (2007).

[26] Heyun Wu; Yonggang Wu; Gang Lv; Zhenhua Wang; Leijie Ling; Zihuan Xia; Naibo Chen. "Preparation and characterization of free-standing Zr, PI and Zr/PI filter", Proc. SPIE 7995, Seventh International Conference on Thin Film Physics and Applications, 79951F (18 February 2011).

[27] M.A. Monclús; M. Callisti; T. Polcar; L.W. Yang; J. Llorca; J.M. Molina- Aldareguía; Selective oxidation-induced strengthening of Zr/Nb nanoscale multilayers; Acta Materialia, 122, 1-10. (2017).

[28] L.R. Doolittle, Nucl. Instrum. Methods B 9, 344, (1985).

[29] A. A. Sokolov; F. Eggenstein; A. Erko, R. Follath; S. Künstner; M. Mast; J. S. Schmidt; F. Senf; F. Siewert; T. Zeschke; F. Schäfers. "An XUV optics beamline at BESSY II", Proc. SPIE 9206, Advances in Metrology for X-Ray and EUV Optics V, 92060J (5 September 2014).

[30] Helmholtz-Zentrum Berlin für Materialien und Energie et al. The At-Wavelength Metrology Facility at BESSY-II, Journal of large-scale research facilities, 2, A50. http://dx.doi.org/10.17815/jlsrf-2-72, (2016).

[31] Nannarone, S; et al., "The BEAR Beamline at Elettra," AIP Conf. Proc. 705, 450 (2004).

[32] Pasquali, L., et al., "The UHV Experimental Chamber for Optical Measurements (Reflectivity and Absorption) and Angle-Resolved Photoemission of the BEAR Beamline at ELETTRA," AIP Conf. Proc. 705, 1142 (2004).

[33] A. Lyapin; L. P. H. Jeurgens; P. C. J. Graat; E. J. Mittemeijer. "The Initial, Thermal Oxidation of Zirconium at Room Temperature," Journal of Applied Physics 96 (12), 7126-7135, (2004).

[34] R.J. Drese; M. Wuttig; "In situ stress measurements in zirconium and zirconium oxide films prepared by direct current sputtering", J. Appl. Phys. 99 (12) 0–5, (2006).

[35] K. Sokhey; S. Rai; G. Lodha. "Oxidation studies of niobium thin films at room temperature by X-ray reflectivity," Appl. Surf. Sci. vol. 257, no. 1, pp. 222–226, (2010).

[36] C.T. Wu. "Intrinsic Stress of Magnetron-Sputtered Niobium Films," Thin Solid Films, vol. 64, pp. 103-110, (1979).